Earth's Future

RESEARCH ARTICLE
10.1029/2025EF006866

Arctic Ozone Hole and Enhanced Mid-Latitude Ozone Losses Due To Heterogeneous Halogen Chemistry Following a Regional Nuclear Conflict

Simchan Yook[1], Susan Solomon[1], Charles G. Bardeen[2], and Kane Stone[1]

[1]Department of Earth, Atmospheric and Planetary Sciences, Massachusetts Institute of Technology, Cambridge, MA, USA, [2]National Center for Atmospheric Research, Boulder, CO, USA

Key Points:

- A regional nuclear war can be expected to cause Arctic ozone holes, due to halogen emissions and smoke chemistry
- Halogen emissions from nuclear war fires and updated heterogeneous chemistry ~ double global ozone loss compared to earlier estimates
- Enhanced UV-B exposure from the ozone depletion after a regional nuclear conflict would pose serious risks to mid-latitude human health

Supporting Information:

Supporting Information may be found in the online version of this article.

Correspondence to:

S. Yook,
syook@mit.edu

Citation:

Yook, S., Solomon, S., Bardeen, C. G., & Stone, K. (2025). Arctic ozone hole and enhanced mid-latitude ozone losses due to heterogeneous halogen chemistry following a regional nuclear conflict. *Earth's Future*, *13*, e2025EF006866. https://doi.org/10.1029/2025EF006866

Received 4 JUL 2025
Accepted 17 NOV 2025

Abstract In a global-scale nuclear war, massive explosions, intense heat, and radioactive fallout would cause extensive harm to humanity and ecosystems. Further, previous studies of even regional-scale nuclear conflicts show that the smoke from large-scale fires caused by such weapons could lead to global-scale ozone loss. However, combustion studies show that urban fires release key ozone-depleting substances that were not previously considered in nuclear war studies, particularly chlorine and bromine compounds. Recent wildfire studies have also shown that high solubility of hydrochloric acid in oxidized organic smoke particles can greatly enhance chlorine-driven ozone loss. For the first time, here we simulate the impacts of a nuclear war on the ozone layer using a chemistry-climate model that accounts for fire-related halogen emissions as well as HCl solubility and heterogeneous chemistry in smoke particles. Our results show that a regional war scenario with 5 Tg of soot could result in a ~40% reduction in the global ozone burden, nearly twice as much as previous studies. The calculated ozone losses exceed ~80% over the Arctic, comparable to those observed when the Antarctic ozone hole was discovered and hence represent an Arctic ozone hole. Ozone losses also reach ~50% over mid-latitudes in the Northern Hemisphere, including highly populated areas. The enhanced ozone loss compared to previous studies is attributable to combined non-linear effects from the incorporation of halogen emissions and updated heterogeneous chemistry in smoke particles. Such ozone losses lead to a large increase in surface ultraviolet exposure, posing grave risks to humanity and ecosystems.

Plain Language Summary Previous research has shown that smoke from large-scale fires ignited by regional-scale nuclear detonations can significantly deplete ozone. Our work expands on this by including emissions of halogen-containing compounds, specifically chlorine and bromine, released from the combustion of urban infrastructure and industrial materials. These halogens can be activated on smoke particles produced by regional nuclear war, becoming highly effective at catalyzing ozone destruction. Using a chemistry-climate model, we find that resulting Arctic ozone reductions could reach levels similar to those of the Antarctic ozone hole, up to ~80%. We also obtain ozone losses of 40%–60% over mid-latitudes, and associated significant increases in surface UV-B radiation. Even a regional nuclear conflict could therefore result in severe ozone depletion and elevated UV exposure, posing serious risks to human health and ecosystems.

1. Introduction

It has been predicted that global nuclear conflicts could have damaging impacts on Earth's climate and ecosystems. Explosions and large-scale fires in urban areas following a global-scale nuclear war between the United States and Russia, for instance, would be expected to generate massive amounts of smoke, released into the atmosphere (Crutzen & Birks, 2016; Glasstone & Dolan, 1977; Lewis, 1979). The smoke aerosol contains black carbon (BC) and would absorb sunlight, heat the ambient air, and self-loft into the stratosphere, where it could remain for several years. This, in turn, would lead to attenuation of the surface solar radiation flux and thus substantial cooling of the surface, sometimes referred to as a "nuclear winter" (Pittock et al., 1985; Robock, 1984; Turco et al., 1983). More recent studies have reproduced these results using modern Earth System models (Robock et al., 2007; Coupe et al., 2019; Bardeen et al., 2021; see also the review by National Academies of Sciences et al., 2022), and studies using climate, crop, and fishery models have also predicted associated global food insecurity and famine in the post-war period due to diminished crop yields resulting from the disruption in climate (Xia et al., 2021, 2022; Xia & Robock, 2013).

Even a much smaller regional-scale nuclear conflict (e.g., a war between India and Pakistan) has been estimated to produce ∼5 Tg of BC particles in the stratosphere and cause global environmental damages, including a significant reduction in the ozone layer (Bardeen et al., 2021; Mills et al., 2008, 2014; Reisner et al., 2018), decreases in global surface temperature and precipitation (Mills et al., 2014; Robock et al., 2007; Stenke et al., 2013; Toon et al., 2007, 2019; Wagman et al., 2020), and widespread food shortages (Xia et al., 2022; Xia & Robock, 2013). Following a regional war involving 5 Tg of BC injection, the global ozone burden has also been predicted to decrease by 20%–25%, while column ozone losses over densely populated regions could be as high as 50%, resulting in 30%–80% increases in summer UV indices over midlatitudes (Bardeen et al., 2021; Mills et al., 2008, 2014; Stenke et al., 2013). For comparison, the 2020 Australian New Year's fires produced 0.3–0.9 Tg of smoke (Peterson et al., 2021; Yu et al., 2021), highlighting the relative magnitude of emissions expected from a regional-scale nuclear conflict.

The stratospheric ozone losses in previous regional nuclear war simulations were primarily driven by large warming due to absorption of solar radiation by nuclear war smoke particles, which in turn increases key reaction rates in the Hydrogen Oxide (HO_x)-catalyzed destruction of ozone, with smaller contributions from similar effects on the Nitrogen Oxide (NO_x) catalyzed reactions and odd oxygen-only (O_x) reactions (Bardeen et al., 2021; Mills et al., 2008). The amount of stratospheric smoke and related ozone loss produced by such a conflict is uncertain and depends, for example, on the details of the weaponry and choice of targets, available fuel at the target sites, geographical location of the conflict regions, how hot the resulting fires are, the BC content of particles produced, whether the particles are subject to wet removal in clouds, and other factors.

Previous modeling studies of the impacts of a regional nuclear war on global ozone loss have not included halogen emissions from the fires (Bardeen et al., 2021; Mills et al., 2008, 2014). However, recent studies on urban and Wildland-Urban Interface fires show that fuel composition in urban and suburban areas differs significantly from that of vegetative biomass in wildlands (Holder et al., 2023; Wang et al., 2025). In particular, urban structures and industrial products contain large amounts of synthetic halogenated compounds (Butler & Mulholland, 2004; Holder et al., 2023; National Academies of Sciences et al., 2022; Wang et al., 2025) that would be released into the atmosphere in the event of fires. More than 10% of the fuel load in modern residential buildings can be comprised of plastics (e.g., nylon or vinyl plank flooring and siding), which often contain chlorine compounds (Blomqvist, P., & Simonson, M., 2009; National Academies of Sciences et al., 2022; Davis & Boundy, 2021; Wang et al., 2025). Vehicles and household items also contain substantial proportions of halogenated compounds, such as polyvinyl chloride (PVC) plastic, and brominated flame retardants are widespread (Holder et al., 2023; National Academies of Sciences et al., 2022; Szewczyński, 2023; Wang et al., 2025). Thus, emissions from various types of fires in urban areas (e.g., waste incineration, open waste burning, and industrial fires) include sizable and readily observable amounts of halogens, especially chlorine and bromine species (Alharbi et al., 2021; Christian et al., 2010; Griffiths et al., 2022; Li et al., 2023; Ni et al., 2016; Zhang et al., 2022). These halogen emissions from urban fires could have significant implications if they reach the stratosphere, since chlorine and bromine catalytically destroy ozone very effectively at those altitudes (Brasseur & Solomon, 2005).

Moreover, recent studies following the 2019/2020 Australian wildfires revealed surprising changes that were unprecedented in the satellite record since 2005 in the distribution of mid-latitude lower stratospheric chlorine species, particularly HCl and $ClONO_2$. Stratospheric ozone also set new record low values at some altitudes in southern midlatitudes in 2020, suggesting substantial depletion. Solomon et al., 2023; Stone et al., 2025 provided evidence that these chemical changes occurred because hydrochloric acid (HCl) is highly soluble in oxidized organics that are routinely observed in smoke particles within a few hours after release into the atmosphere. The enhanced HCl solubility leads to heterogeneous chemistry similar to that observed in the Antarctic on the surfaces of Polar Stratospheric Clouds (PSCs), but at much warmer mid-latitude temperatures. Estimates from previous studies suggest that fires in urban areas could emit organic carbon (OC) along with BC (sometimes called soot) accounting for up to ∼30% of total smoke emissions (Andreae, 2019; Dod et al., 1989; Reisen et al., 2014), supporting a potential for increased heterogeneous chemistry in organics in the stratosphere.

Building on new findings concerning halogen and OC emissions and their role in halogen activation, we use a climate-chemistry model to simulate the impacts of regional-scale nuclear wars on global climate and the ozone layer. For the first time, nuclear war scenarios are simulated with updated stratospheric chemistry including the effects of smoke particles on heterogeneous halogen reactions and with additional injection of chlorine and bromine from urban fires to the stratosphere. The following section (Section 2) describes the model, emission

inventory, and scenarios. Section 3 probes the impacts of regional nuclear conflict on global climate and the ozone layer, and Section 4 presents a discussion and summary of the results.

2. Model and Scenarios

To assess climate responses to a regional nuclear conflict, Bardeen et al. (2021) used simulations conducted with a coupled chemistry-climate model that includes stratospheric ozone chemistry and Tropospheric Ultraviolet and Visible (TUV) radiation calculations (Madronich & Flocke, 1997). Our simulations closely follow the methods outlined in Bardeen et al. (2021); we further add halogen and OC emissions, and we also consider the solubility of HCl in OC particles and resulting heterogeneous chemical reactions.

2.1. Aerosol and Gas Emissions

Fuel estimation in this study follows the regional nuclear exchange scenario from Toon et al. (2007, 2019), which assumes a war between India and Pakistan lasting 4 days and burning a total of 250 Tg of urban fuels. Toon et al. (2007, 2019) estimated that such a regional nuclear war could generate 5 Tg of BC aerosol particles in the upper troposphere. Following their estimates, smoke particles in our simulations are injected into the upper troposphere, rather than at the surface, with a constant mixing ratio between 150 and 300 hPa over urban targets in India and Pakistan during 12–15 January of the first simulation year. All other gases from surface fires are also assumed to be initially emitted at the same location and time as the smoke particles. This assumption is consistent with those used by Mills et al. (2008, 2014) and Bardeen et al. (2021). The locations of the urban targets emitting smoke plumes are shown in Figure S1 in Supporting Information S1.

2.1.1. Smoke Emissions

The Community Aerosol and Radiation Model for Atmospheres (CARMA; Bardeen et al., 2008; Toon et al., 1988) is used to simulate BC and OC aerosols in this study. CARMA is a sectional microphysics model that governs prognostic aerosol processes including coagulation, wet and dry deposition, and gravitational settling in a size-resolved manner. The structure of BC particles is represented by a fractal morphology, consisting of clusters of uniformly sized spheres. A monomer radius of 30 nm is assumed, along with a fractal dimension of 2.2 and a packing coefficient of 1.3 for the aerosol size distribution (Bardeen et al., 2021; Wolf & Toon, 2010). This approach using CARMA for soot representation follows Bardeen et al. (2017, 2021) and has been applied in previous studies of nuclear war (Coupe et al., 2019; Toon et al., 2019).

Smoke is a complex mixture of soot (BC) and different organic compounds (Toon et al., 2019). In this study, we assume a composition of 70% BC and 30% OC (i.e., 5 Tg BC and 1.66 Tg OC), rather than treating smoke as pure BC. The sensitivity of the climate response to different BC/OC mass ratios will be examined in a separate study.

2.1.2. Nitrogen Oxide (NO_x) Emissions

Nitrogen Oxide (NO_x), a mix of nitric oxide (NO) and nitrogen dioxide (NO_2), can be produced by a nuclear explosion through two main pathways (for details, see Bardeen et al., 2021):

1. formation in the fireball of the explosion, with an assumed emission rate of 1×10^{32} molecules of NO per megaton (Mt) of yield (National Resource Council, 1985), and
2. emission from the resulting fires, with an estimated emission rate of ~2 g of NO_x per kg of fuel burned (Andreae, 2019).

The total NO_x emissions in our simulations include contributions from both the fireball and the resulting fires. Again, all particles and gases from the fires are injected into the upper troposphere over 3 days, following the war scenario described in Section 2.1. However, NO from the fireball is released on the first day of the war and emitted uniformly between the top and bottom of the fireball (see Section 2.4.1 in Bardeen et al., 2021, for details on fireball height calculations). For simplicity, NO_x is emitted in the model only as NO, since NO and NO_2 rapidly interconvert (Brasseur & Solomon, 2005), making the distinction in initial emission unimportant.

Table 1
Comparison of Chlorine and Bromine Emission Factors From Urban Fuels Across Different Data Sources

Unit: (g/kg)	Structures					Vehicles			
Cl	3.2	3.56			2.5				
HCl		11	0.5–1.3	6–18		11	6.4	1.8	
Br				0.0053					0.26
HBr					0.321				0.11
Reference	Zhang et al. (2022)	Holder et al. (2023)	Blomqvist et al. (2010)	Gann et al. (2010)	Holder et al. (2023)	Holder et al. (2023)	Lönnermark and Blomqvist (2006)	Text S1.2 in Supporting Information S1	Holder et al. (2023)

2.1.3. Halogen Emissions

Fuel loadings from urban fires—resulting from the burning of structures, vehicles, and their contents—have very different compositions compared to fuels from wildfires. One of the key differences is their halogen content. Plastics composites including PVC, which contains chlorine, constitute approximately 10% of the total mass of modern residential buildings and vehicles (Blomqvist, P., & Simonson, M., 2009; National Academies of Sciences et al., 2022; Davis & Boundy, 2021) and are emitted mainly as HCl in fire smoke. Wildfires, by contrast, have much smaller amounts of chlorine in their fuel-loading makeup (Andreae, 2019). According to Holder et al. (2023), the emission factor for HCl is three orders of magnitude greater for urban fuels than for biomass fuels. In this study, we assume that the regional nuclear war leads to fires in highly populated urban areas.

Table 1 lists the chlorine and bromine emission factor data used to characterize urban fires from multiple sources, along with all references supporting these Cl and Br emission estimates. Supporting Information S1 provides details on how the emission factors for the simulations were computed. Chlorine emission factors range from 2.5 to 3.56 g per kilogram of fuel burnt (g/kg) for particulate Cl and from 0.5 to 11 g/kg for HCl, with some studies measuring both of these but others measuring only one; there is thus a wide range and consistency only roughly in order of magnitude across the literature. The sum of particulate and gas phase HCl (total chlorine) might be as high as about 15 g/kg or as low as 3. Similarly, bromine emission factors range from 0.005 to 0.260 g/kg for particulate Br and from 0.11 to 0.321 g/kg for HBr, implying total bromine ranging from as low as 0.12–0.58 g/kg. Using these multiple sources, we estimate approximate best guesses for emission factors of 11 g/kg for total chlorine and 0.32 g/kg for total bromine (see Supporting Information S1 for details). These correspond to total emission of ∼3 Tg of chlorine and 0.08 Tg of bromine in the baseline 5 Tg soot injection scenario. The chlorine emission value was rounded up from 2.75 Tg for simplicity. As a key sensitivity test, we also consider a case with 1.5 Tg of chlorine and 0.04 Tg of bromine as a lower-emission scenario. Note that the baseline scenario is referred to as the 5 Tg soot injection scenario, following the naming convention used in previous nuclear war modeling studies. However, the total mass of the smoke plume—including BC, OC, and other emitted gases—in this study is closer to ∼10 Tg.

Some uncertainties remain in the estimation of halogen emissions due to variations in measurement techniques and other factors, such as differences in fuel inventories and fuel types across data sources. To further illustrate sensitivity to uncertainties in halogen emission rates, a range of halogen emission scenarios at different scales has also been tested. For simplicity, halogen was only emitted in the model as gas-phase Cl and Br. Both species should rapidly convert to other forms and between gas and particulate phases following atmospheric chemistry; for example, Cl is rapidly converted to HCl throughout much of the atmosphere, so the effect of the initial partitioning between Cl and HCl should be small.

We note that Cl and HCl are often measured separately as distinct emission sources using different methods in fire emission studies (see for in Supporting Information S1.1. For further information).

2.2. Model

2.2.1. WACCM4 Model

The Whole Atmosphere Community Climate Model Version 4 (WACCM4; Marsh et al., 2013) of the Community Earth System Model (CESM; Hurrell et al., 2013) is used in this study. The WACCM simulations are run with a

horizontal resolution of 1.9° × 2.5°, 66 vertical levels, a model top at about 140 km, coupled to interactive ocean, land, and sea ice models. The chemistry scheme used in WACCM4 is based on version 3 of the Model for Ozone and Related Chemical Tracers (Kinnison et al., 2007), which includes detailed chemistry for the middle and upper atmosphere. The chemistry module includes a total of 59 chemical species contained where appropriate in the O_x, NO_x, HO_x, ClO_x, and BrO_x chemical families, along with 217 gas-phase reactions and 17 heterogeneous chemical reactions, capturing all the key processes involved in ozone hole formation. To update the chemistry in line with current standard WACCM simulations, we reduced the nitric acid trihydrate particle number density from 10^{-2} to 5.0×10^{-4} cm^{-3} following Weimer et al. (2023) and replaced the prescribed sulfate aerosol input with a time series of climatological monthly means (2000–2020) from a ten-member fully coupled WACCM ensemble (Garcia et al., 2017). This fully coupled chemistry-climate configuration of CESM-WACCM is well suited to assess surface climate responses and air temperature changes resulting from the radiative forcing of nuclear conflict emissions, along with their impacts on chemical reactions.

The large aerosol burdens in the nuclear war scenario act as significant climate perturbations, leading to substantial temperature increases in the stratosphere. These air temperature increases are up to 30°C in the global average (so large that they required model modifications to improve numerical stability), and they affect the kinetic rates of chemical reactions (particularly those with large energies of activation). Details of these changes and the model setup are provided in the Supporting Information of Bardeen et al. (2017).

In prior nuclear war studies using WACCM4, the actinic flux required for calculating photolysis rates was estimated using a lookup table. Thus, the photolysis rates did not account for the direct effects of added aerosol scattering and absorption due to nuclear emissions. For the current study, version 4.2 of the TUV model (Madronich & Flocke, 1997) was incorporated to provide an in-line calculation of actinic flux. This approach accounts for actual O_3, SO_2, and aerosol profiles, allowing for a better representation of photolysis rates. Additionally, TUV can output spectral integrals of useful radiative fluxes, such as UV-B and photosynthetically active radiation, which can help assess the atmospheric impacts on ecosystems. Further details of the TUV calculations are provided in Bardeen et al. (2021).

2.2.2. Updates Accounting for the Role of Organic Particles on Stratospheric Chlorine Chemistry

In addition to the model updates discussed above, we have also updated the heterogeneous chlorine chemistry to incorporate HCl solubility on OC surfaces, which is a feature does not present in the standard version of WACCM4. HCl solubility is a key factor in stratospheric heterogeneous chemistry because the rates of heterogeneous reactions involving chlorine depend on the molarity of HCl within liquid aerosols (Solomon et al., 2023; Stone et al., 2025). At midlatitude stratospheric temperatures, aerosols are typically composed of sulfate and water, which are too acidic to allow much HCl to dissolve, limiting the rates of these heterogeneous reactions. However, laboratory measurements show that HCl is far more soluble in organic species than in sulfate aerosols at relatively warm stratospheric temperatures. Accounting for the high HCl solubility in stratospheric organic aerosols from the 2020 Australian wildfires led to extreme HCl and $ClONO_2$ anomalies not previously seen in the satellite record since 2005, and accompanying ozone depletion in the midlatitude stratosphere that aligned well with observations (Solomon et al., 2023).

Based on the high HCl solubility in organic species reported by Solomon et al. (2023), the following assumptions are made in our simulations. Nuclear emissions of BC and OC are treated as homogeneously mixed within the CARMA mixed carbon bins. We assume that these mixed carbon aerosols dissolve HCl similarly to pure organics, following evidence for liquid-liquid phase separation (see Stone et al., 2025 and references therein). The high HCl solubility in organics is applied whenever the ratio of the nuclear carbon particle surface area density to that of background sulfate particles exceeds 1 (Stone et al., 2025); otherwise, HCl solubility follows the standard parameterization in sulfate aerosol (Shi et al., 2001). This simplification is valid given the substantially larger amount of carbon-containing particles from the nuclear fires compared to background sulfate aerosols during the first few years of the simulations. Sensitivity experiments to test the impact of this updated HCl solubility in organic aerosols are also conducted, as described in the following sections.

In addition to incorporating HCl solubility in OC, the surface area density function used in heterogeneous chemistry has been updated to include smoke particles. This modification influences other heterogeneous processes, including N_2O_5 hydrolysis. Solomon et al. (2023) investigated N_2O_5 hydrolysis following the wildfires and concluded that it likely occurred on fire aerosols as well, supporting this modification.

Table 2
List of the WACCM4 Experiments With Different Emission Scenarios

Scenario	Species added	Updated heterogeneous chemistry Y/N
CTRL	–	Y
IP	Smoke (BC/OC)	Y
IP-BR	Smoke (BC/OC), Br	Y
IP-CL	Smoke (BC/OC), Cl	Y
IP-NO	Smoke (BC/OC), NO	Y
IP-ALL	Smoke (BC/OC), Br, Cl, NO	Y
IP-NO-xHET	Smoke (BC/OC), NO	N
IP-ALL-xHET	Smoke (BC/OC), Br, Cl, NO	N

2.2.3. Experiments

We conducted three sets of WACCM simulations. Each set of experiments is designed to explore the sensitivity of climate responses to different types of forcing or chemistry as follows:

1. Different emission scenarios from nuclear war fires

The first set of experiments assesses the climate response to different combinations of gases and aerosol emissions resulting from nuclear war fires: (a) **CTRL** scenario, the control experiment without any nuclear emissions, and (b) India-Pakistan (**IP**) scenarios, five perturbed experiments run with different types of nuclear emissions based on the **IP** conflict scenario. Each perturbed scenario is named **IP** (which indicates the scenario includes BC/OC emissions from regional nuclear conflicts) followed by a specific type of gas emission. For example, **IP** denotes the simulation run with emissions of black and OC only, while **IP-NO** includes these emissions along with NO emission. Details of the emissions used in the **IP** runs are presented in Table 2.

2. Role of updated heterogenous chemistry

The second set of experiments explores the sensitivity of results to the inclusion of updated heterogeneous chemistry. Experiments without the updated heterogeneous chemistry are labeled with the suffix "**-xHET**" after the emission-based scenario naming convention.

For example, **IP-ALL-xHET** refers to a simulation with all emissions, including halogens, but without updated chemistry on organic surfaces, and **IP-NO-xHET** includes only NO emissions and excludes the updated heterogeneous chemistry.

In the **IP-NO-xHET** experiment, the NO_x and smoke emissions are consistent with the **IP-NO** simulations described in Bardeen et al. (2021), except that we assumed the OC content represented 30% of the total smoke mass to ensure consistency with other new experiments in the current study. Thus **IP-NO-xHET** run serves as a reference case that allows for comparison with results from previous studies. It can also be compared with the **IP-NO** run to estimate the impact of heterogeneous chemistry in organics on stratospheric chemistry in the absence of additional halogen emissions.

The difference between **IP-ALL-xHET** and **IP-NO-xHET** reveals the role of the added halogen species from the nuclear fires but without updated heterogeneous chemistry in organics, while the difference between **IP-ALL** and **IP-ALL-xHET** isolates the role of heterogeneous chemistry in smoke organics on stratospheric chemistry in the nuclear war experiments with halogen emissions.

3. The Magnitude of Halogen Emission

The third set of experiments evaluates the sensitivity of results to uncertainties in halogen emission estimates. Relative to the **IP-ALL** scenario, Cl and Br emissions were scaled by factors of 0.125, 0.25, 0.5, 0.75, and 1.5, with each run labeled **IP-ALL-EmisScale0.125** through **IP-ALL-EmisScale1.5**.

All experiments are run for 3-year long. Although the simulation was conducted using a single ensemble member, the amplitudes of the responses to the imposed perturbation exceed those of typical internal climate variability, allowing for a robust interpretation of the results.

3. Results

3.1. Global Climate Responses to a Regional Nuclear Conflict

Figure 1 shows the responses to different emission scenarios associated with the IP conflict, including changes in (a) stratospheric temperature and (b) global total column ozone. All **IP** runs exhibit substantial warming of the global stratosphere, characterized by a rapid increase in temperature exceeding ∼10 K within the first two months and peaking at approximately 15 K during the first half of the year (Figure 1a). This warming is primarily driven by the absorption of shortwave radiation by the injected smoke particles and is consistent with the results from previous studies (Bardeen et al., 2021; Mills et al., 2008, 2014; Robock et al., 2007). The temperature anomalies gradually decrease as smoke is removed from the atmosphere over time.

Note that the globally averaged total column ozone, expressed in Dobson Units (DU), can be directly converted to the global ozone burden. e.g., a global mean value of 1 DU, when multiplied by Earth's surface area, corresponds to approximately 10.3 Tg of ozone. Thus, a TCO of ∼300 DU corresponds to a global ozone burden of ∼3,280 Tg. Therefore, we use the terms global total column ozone and global ozone burden interchangeably. The global ozone burden in all **IP** simulations shows peak decreases ranging from 20% to 40% by the end of the second year. Simulations exhibiting more pronounced ozone loss (e.g., **IP-ALL** and **IP-CL** runs shown as red and green lines, respectively) in Figure 1b show reduced stratospheric warming (Figure 1a) due to decreased absorption of shortwave radiation by stratospheric ozone. These ozone differences are discussed in more detail below.

In simulations without halogen emissions (i.e., the **IP**, **IP-NO**, and **IP-NO-xHET**) the global ozone burden is projected to decline by ∼20%, which is consistent with previous estimates from regional nuclear war simulations. In these experiments, ozone depletion is mainly due to stratospheric warming and the temperature dependencies of ozone loss reactions, as discussed in earlier work (Bardeen et al., 2021; Mills et al., 2008, 2014). The ozone loss in the **IP-NO** and **IP-NO-xHET** runs shows little difference. By design, the only difference between these two simulations is the inclusion of heterogeneous chemistry on organic particles in the **IP-NO** run. Thus, the small differences in ozone depletion between the **IP-NO** and **IP-NO-xHET** runs indicate that, in the absence of additional urban fire-related halogen emissions, ozone loss in our nuclear war scenario is not significantly affected by heterogeneous chemistry on OC particles. We note that the peak of our calculated nuclear fire aerosol is located near 20 hPa, which is potentially sensitive to the choice of aerosol and radiation scheme. Consequently, this result may depend on both the model and the specific war scenario, including the geographic locations of the nuclear conflicts.

Two key distinctions between our simulations and prior regional nuclear war studies are: the inclusion of (a) halogen emissions from urban fires and (b) updated heterogeneous chemistry on organic aerosol surfaces. To elucidate the impact of these changes on ozone loss, we compared the **IP-ALL** simulation (which includes both) with the **IP-NO-xHET** simulation (which omits both), where the latter is consistent with the simulation setups used in previous studies.

We defined peak ozone loss as the ozone levels when the global ozone burden reaches its minimum during October–December (OND) of the first year and January-March (JFM) of the second year. The **IP-ALL** scenario revealed a peak global ozone loss of 38%, representing a substantial increase (∼140%) in ozone loss compared to the 16% loss in the **IP-NO-xHET** scenario. The **IP-ALL-xHET** experiment, which included the halogen emissions but not the updated organic aerosol chemistry, resulted in 26% global ozone loss. While the **IP-ALL-xHET** run showed greater relative ozone loss than the **IP-NO-xHET** run, its peak ozone depletion was significantly smaller than that in the **IP-ALL** run. Thus, in the absence of updated heterogeneous chemistry, gas-phase chemistry including additional nuclear war halogens play a limited role in driving the stratospheric ozone depletion. Note that taken together with the results from the **IP-NO** and **IP-NO-xHET** runs, the results indicate that the impact of halogen chemistry on ozone loss is not a linear sum of halogen emissions (i.e., difference between the **IP-ALL** and **IP-ALL-xHET** runs) and heterogeneous chemistry effects (i.e., difference between the **IP-NO** and **IP-NO-xHET** runs), but rather arises from their combined, nonlinear effects. These findings highlight

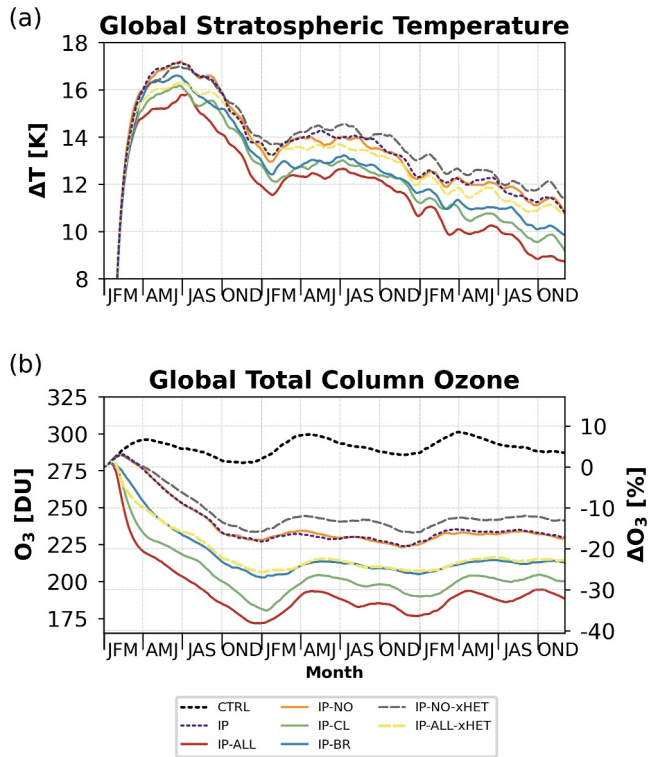

Figure 1. Time series of (a) global stratospheric temperature and (b) global total column ozone from simulations with different emission scenarios. Temperatures in **IP** runs are shown as anomalies relative to the **CTRL** run, highlighting the differences between the **IP** and **CTRL** simulations. Percent anomalies in ozone are defined relative to the initial ozone abundances (278 DU) on January 1 in the **CTRL** run. For graphical purposes, a 30-day running mean was applied to panel (a). The global stratospheric temperature anomaly represents the change in the density-weighted vertical average of temperature above the tropopause level. Horizontal gray lines represent 2 K interval of global stratospheric temperature in panel (a) and 10% interval of the percentage changes in ozone in panel (b), respectively.

the importance of both halogen emissions and heterogeneous chemistry on organic aerosols for accurately simulating ozone loss.

The **IP-ALL**, **IP-CL**, and **IP-BR** experiments show peak global average ozone losses of 38%, 35%, and 27%, respectively (Figure 1b). Compared to the global ozone loss in the reference scenario (**IP**, 19%), the combines losses from the single-halogen scenarios (16% for **IP-CL** and 8% for **IP-BR**) are ∼5% larger than the net ozone loss in the combined-emissions experiment (**IP-ALL**). Although cross-cycle chemistry between ClO_x and BrO_x species would be expected to enhance ozone loss in the **IP-ALL** experiment, the results suggest that ozone saturation occurs, such that the net ozone loss in **IP-ALL** is not greater than the linear sum of ozone losses in **IP-CL** and **IP-BR**. The details of ozone loss saturation under different levels of halogen emission scenarios are discussed in the following section.

Figure 2 illustrates the sensitivity of ozone loss to halogen emission rates by presenting results from simulations run with varying amounts of halogen emissions. The simulations are run with the same emission rates as in **IP-ALL**, but with both chlorine and bromine emissions scaled by different factors ranging from 0.125 to 1.5. To highlight the difference in ozone loss solely due to halogen emissions, the ozone anomalies are defined as deviations from the **IP-NO** runs in Figure 2. The rate of increase in peak loss of the global ozone burden (Figure 2a) appears to slow at higher emission scenarios, suggesting that saturation occurs. For instance, the **IP-ALL** scenario resulted in extra ∼56 DU of globally averaged total column ozone loss compared to the **IP-NO** scenario without any halogen emissions, whereas the **IP-ALL-EmisScale0.5** scenario, which utilizes half the halogen emissions, resulted in an additional ∼38 DU of ozone loss. Thus, the additional ozone loss in the **IP-ALL** scenario is smaller than the linear scaling implied by the difference between the **IP-ALL-EmisScale0.5** and **IP-NO** runs (which

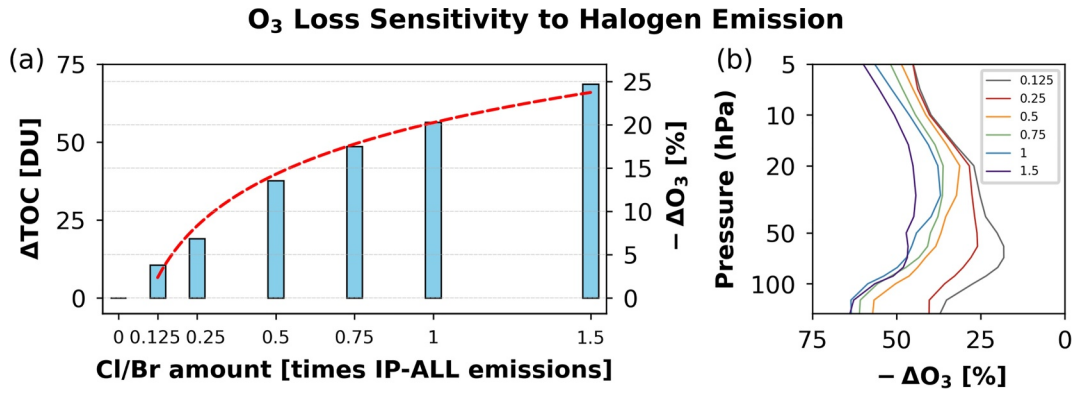

Figure 2. (a) Peak loss of global ozone burden and (b) vertical profile of peak ozone loss in simulations with varying intensity of halogen emissions. Peak ozone loss is defined as in Figure 1. Ozone anomalies are defined as deviations (a) from the **IP-NO** simulation and (b) from the **CTRL** simulation, respectively. Percent anomalies of ozone concentration (unit: number density, molecules/cm^3) are normalized by the initial ozone concentration on January 1 in the **CTRL** run.

would be 38 × 2 = 76 DU). Nevertheless, the results from **IP-ALL** represent a substantial 40% net reduction in global ozone burden due to the nuclear war forcing.

Figure 2b shows the vertical profiles of the ozone concentration anomalies (unit: number density, molecules/cm^3) in the different scenarios, and indicates that the saturation effect comes at lower altitudes (below about 50 hPa). Figure S2 in Supporting Information S1, which presents ozone loss in units of number density rather than percentage anomalies, reveals a similar vertical structure of ozone loss saturation below ∼50 hPa. The ozone losses are close to 100% at some latitudes near 100 mb for high levels of added chlorine (implying saturation) but are much smaller in the deep tropics (around 30%), so that the global mean loss at this level peaks near 70% (Figure 2b). These latitudinal differences of the ozone losses are examined further in Figure 3.

We also tested a different injection date of 12–15 July (**IP-ALL-SUMMER** experiment). The seasonality of the injection in that case does not qualitatively affect the longer-term behavior of the results (Figure S3 in Supporting Information S1), but the stratospheric warming and ozone losses in the first winter were smaller than in the **IP-ALL** experiment.

Polar regions typically offer more favorable conditions for ozone loss than midlatitudes, primarily due to cold temperatures and the formation of PSCs (Solomon, 1999). Figure 3a displays the column ozone burden for the

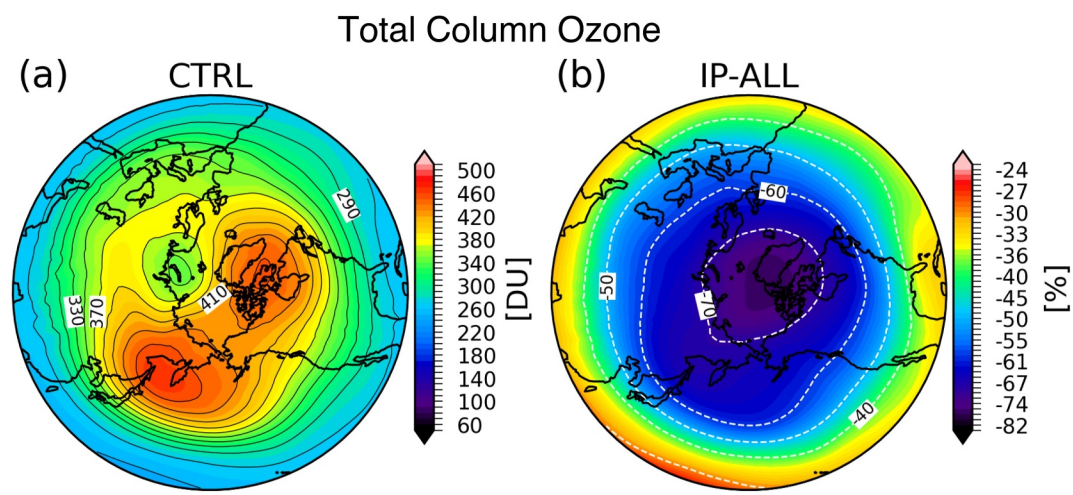

Figure 3. Northern Hemisphere column ozone from (a) **CTRL** run, and (b) percentage ozone loss in **IP-ALL** relative to the **CTRL** run. Ozone values are averaged from January to April of the second year. Note that contour levels in panel (b) are logarithmically spaced.

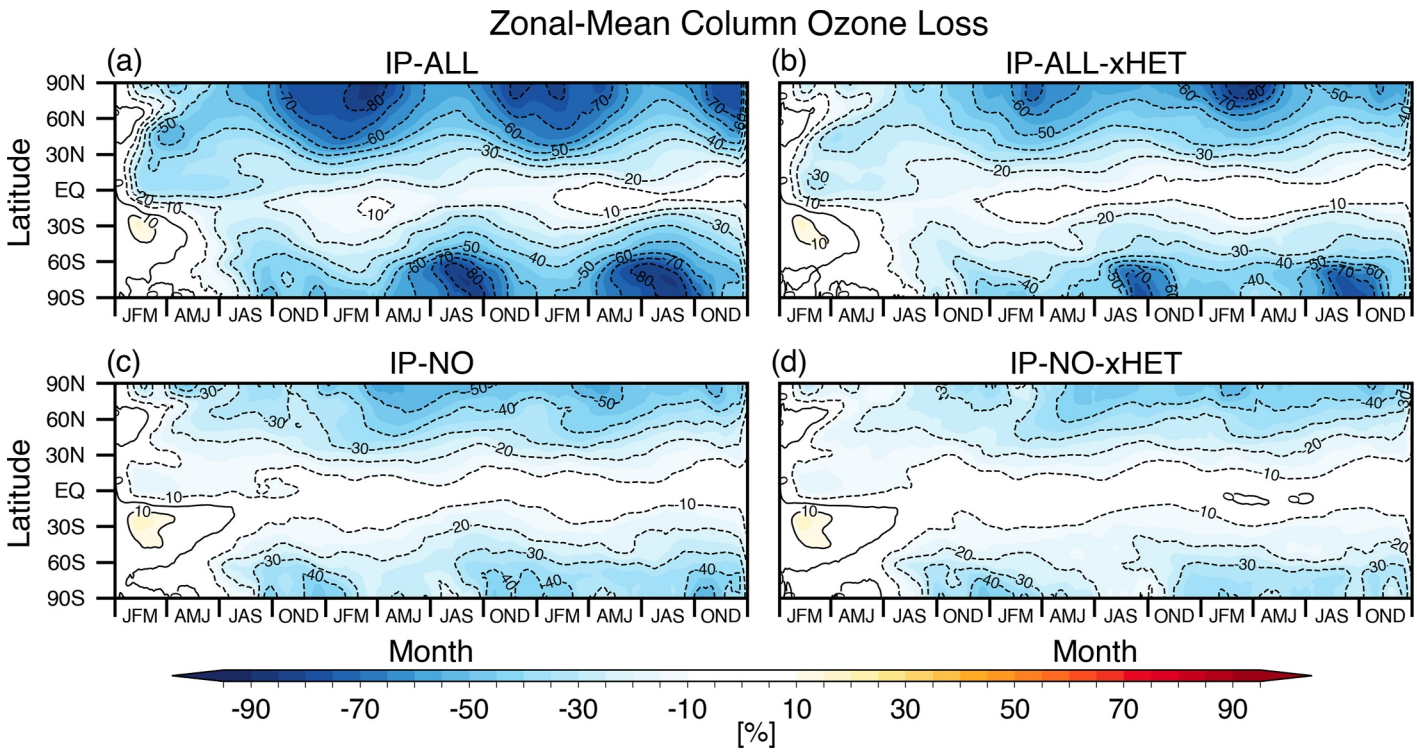

Figure 4. Changes in zonal-mean total column ozone as a function of latitude and time, relative to the **CTRL** simulation, from (a) **IP-ALL** run, (b) **IP-ALL-xHET** run with halogen emission but using the previous version of heterogeneous chemistry as in Bardeen et al. (2021), (c) **IP-NO** run without halogen emission, and (d) **IP-NO** without halogen and the updated heterogeneous chemistry. A 30-day running mean was applied.

CTRL run over the Northern Hemisphere (NH) averaged from January to April of the second year. The NH column ozone burden over the extratropics and high latitudes ranges from ~300 to 450 DU, generally increasing with latitude. Similarly, Figure 3b shows column ozone difference between **IP-ALL** and **CTRL** runs. The results in Figure 3b indicates that the nuclear war scenario leads to significant decreases in column ozone across the NH. By far the most pronounced total column ozone losses are observed over the polar regions, with peak losses reaching ~80% of the total column. In the real world, October ozone depletion in the Antarctic is typically about 70% of the total column in years of high depletion compared to unperturbed pre-ozone hole conditions (see, e.g., the review by Solomon, 1999). Therefore, the large losses of total ozone obtained in our **IP** simulations can reasonably be called an "Arctic ozone hole."

Figure 4a further explores the latitudinal and seasonal pattern of column ozone loss between the **IP** and **CTRL** runs. The results from the **IP-ALL** run show pronounced ozone losses: (a) over mid-latitudes (30–60°N) in the first few months and (b) repeating losses over mid-latitudes and polar regions during winter/spring seasons (Figure 4a). The substantial ozone losses following the **IP-ALL** scenario are not limited to the north polar region. Instead, they are also occurring over mid-latitudes, including the conflict zones at the edge of the tropics where the nuclear emissions were initially injected but also at higher latitudes in both hemispheres near 45–60° later in the simulations, around November–December. Total ozone losses in the mid-latitude region for the **IP-ALL** run are about 40%–60%.

Figures 4b–4d compare the sensitivity of ozone loss to halogen emissions and to updates in the heterogeneous chemistry in OC particles. For example, the results in Figure 4d represent ozone loss from the reference simulation (**IP-NO-xHET**), which was run without halogen emissions and used the standard version of heterogeneous chemistry as in Bardeen et al. (2021). Figures 4b and 4c show results from simulations with halogen emissions but without the updated chemistry (**IP-ALL-xHET**), and with the updated chemistry but without halogen emissions (**IP-NO**), respectively.

The **IP-ALL-xHET** experiment with nuclear war halogen emissions shows excessive ozone losses in the polar regions during the winter/spring seasons (Figure 4b), as observed in the **IP-ALL** experiment (Figure 4a). This

highlights the role of halogen input and enhanced heterogeneous halogen chemistry in driving the springtime polar ozone depletion. All these sensitivity experiments show much smaller ozone losses (Figures 4b–4d) than **IP-ALL** and lack the initial mid-latitude ozone depletion observed in the **IP-ALL** run (Figure 4a). This marked difference between **IP-ALL** and the sensitivity experiments highlights the important roles of combined non-linear effects from the (a) added halogen inputs and (b) the updated heterogeneous chemistry in driving the large ozone losses seen in the **IP-ALL** run.

Together, the results presented in Figures 1–4 demonstrate two key findings, (a) regional nuclear conflict emissions can cause substantial changes in atmospheric temperature and ozone, even resulting in an Arctic ozone hole as well as substantial mid-latitude losses and (b) implementation of halogen emissions combined with heterogeneous chemistry in OC significantly enhances the simulated ozone loss.

3.2. Role of Nuclear War Emissions, Chemical Cycles, and Atmospheric Processes in Global Ozone Depletion

In this section, we assess the detailed role of different chemical reactions in driving the substantial ozone loss. We focused on the **IP-ALL** simulation to examine the scenario with the largest ozone depletion. Figure 5 provides a general overview of changes in various atmospheric fields and chemical species from the **IP-ALL** simulation. The BC/OC aerosol mixing ratio (Figure 5a) exhibits a marked enhancement in the lower-to-mid stratosphere, resulting from rapid self-lofting of the aerosol plume within the first few days following injection. This lofted aerosol layer remains well above the tropopause throughout the simulation period. The temporal evolution of the smoke plume is also shown in Figure S4 in Supporting Information S1. Over the 3-year simulation period, the BC/OC aerosol was removed from the stratosphere at an average rate of ∼1.2 Tg yr^{-1}, from an initial peak burden of ∼5.7 Tg. By the end of the first year, the stratospheric soot burden had declined by ∼30%. While aerosol lifetime affects both the intensity and persistence of climate impacts following a nuclear conflict, our analysis primarily focuses on peak ozone depletion in the first year. Thus, we consider the influence of these differences to be relatively minor. Further discussion of the relationship between particle size and lifetime time is provided in Bardeen et al. (2021). The aerosol leads to substantial warming in the stratosphere (Figure 5b), with temperature anomalies reaching several tens of kelvins throughout the stratosphere. The warming peaks at approximately 30 K near the 30 hPa level.

This thermodynamic and chemical responses to the nuclear emission modify the chemical composition and the water vapor content in the stratosphere. The ozone concentration (Figure 5c) shows a pronounced decrease between the 10–50 hPa levels, overlapping with the regions of maximum aerosol loading and stratospheric warming. The specific humidity (q, shown in Figure 5d) exhibits a substantial increase in the lower stratosphere, consistent with the well-known effect of tropopause warming, which facilitates enhanced water vapor transport into the lower stratosphere (Jensen & Pfister, 2004; Mills et al., 2014).

The bottom row of Figure 5 shows changes in key reactive chemical species relevant to ozone chemistry. The NO_x concentration exhibits a decrease around ∼20 hPa, juxtaposed with an increase above ∼5 hPa. We note that our results differ slightly from those of Bardeen et al. (2021), which did not show a mid-stratospheric decrease in NO_x. These differences arise from heterogeneous chemistry involving NO_x in our simulations (particularly hydrolysis of N_2O_5 on the enhanced aerosol concentrations), as discussed in more detail in a later section. The HO_x concentration (Figure 5f) increases throughout the stratosphere, potentially contributing to ozone loss. The reactive halogen species, ClO and BrO (Figures 5g and 5h), also exhibit pronounced increases in concentration, which can be expected to enhance ozone loss through catalytic cycles. Note that the changes in ClO, in units of number density, also exhibit a qualitatively similar pattern to that in Figure 5g, but with less saturation in Figure S5 in Supporting Information S1. The pronounced saturation in Figure 5g arises from the low background ClO at these altitudes in the **CTRL** experiment (Figure 5a).

Figure 6 summarizes the changes in the vertical distribution of the global ozone (unit: number density, molecules/cm^3) and the associated odd-oxygen chemical reaction rates. Here we focus on the first year, as the largest changes in global ozone abundance occur during the first year (Figure 1). Again, significant decreases in the global ozone concentration are shown throughout most of the stratosphere (Figure 6a). The "odd-oxygen" family includes ozone and related species involved in rapid chemical cycles, and the figure represents the major sinks of ozone. The definitions of each odd-oxygen production and loss rate in WACCM4 are provided in Table 2 of Bardeen et al. (2021). Net odd-oxygen loss rate shows a pronounced increase (over 250%) in the stratosphere in the **IP-**

10.1029/2025EF006866

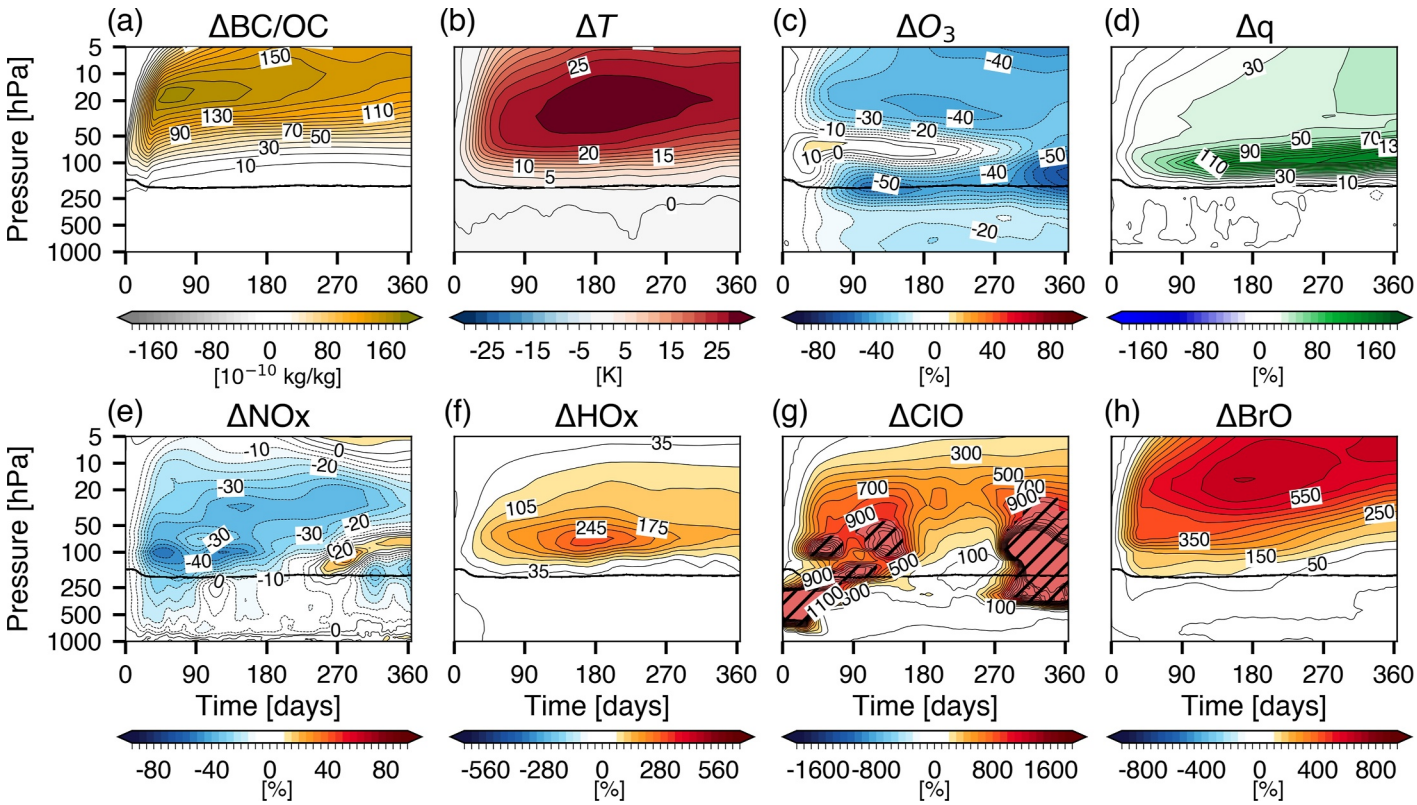

Figure 5. Changes in globally averaged fields of (a) smoke particle, (b) temperature, (c) ozone, (d) specific humidity, (e) NOx, (f) HOx, (g) ClO, and (h) BrO between the **IP-ALL** and **CTRL** runs. The changes are calculated as a function of level and time during the first year of the simulation. A 30-day running mean was applied. Black line in Figures 5, 7, and 8 denotes the tropopause height. In panel (g), the regions where the % increase exceeds 1,000% are masked out.

ALL run compared to the **CTRL** run (Figure 6b). The halogen cycles (ClO_x and BrO_x) account for the largest fraction of this increase in net loss rate, while the HOx cycle also contributes, but to a lesser extent. These results confirm that halogen emissions from the nuclear war scenario are the primary driver of ozone loss through their catalytic cycles.

Note that ozone abundance change in the lower stratosphere shows a local minimum around the ~70 hPa level, even though the largest increase in chemical loss rate occurs at similar altitudes (Figure 6). This smaller decrease in ozone abundance is attributed to dynamical ozone transport associated with circulation anomalies, consistent

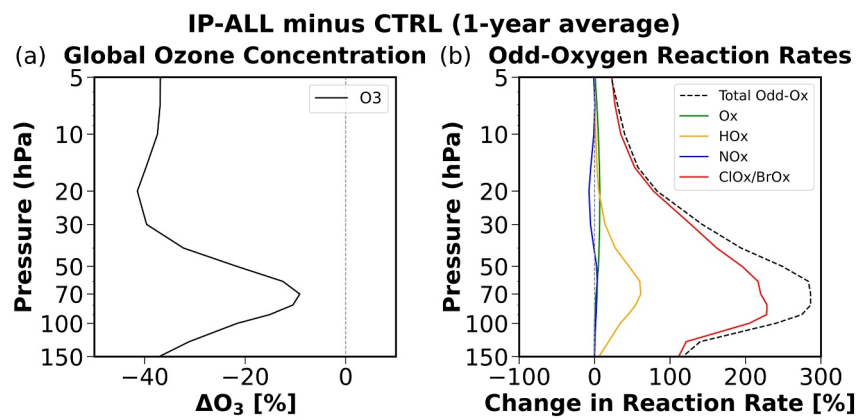

Figure 6. Changes in global average vertical profile of (a) ozone and (b) odd-oxygen loss rates between the **IP-ALL** and **CTRL** runs. The results focus on the first year, during which the largest changes in global ozone burden occur. The gray dashed line in panel (a) denotes zero for reference.

10.1029/2025EF006866

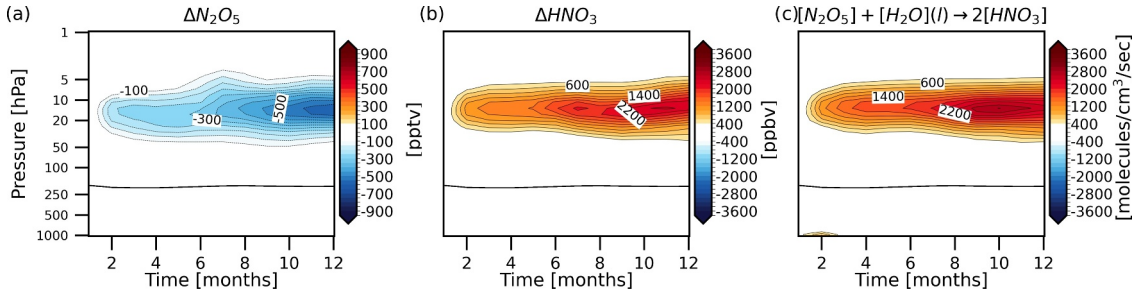

Figure 7. Changes in (a) N_2O_5, (b) HNO_3, and (c) reaction rate for heterogeneous conversion of N_2O_5 to HNO_3 between the runs with (**IP-ALL**) and without (**IP-ALL-xHET**) updated heterogeneous chemistry.

with the weakening of tropical upwelling in the Southern Hemisphere's lower tropical stratosphere (Figure S6 in Supporting Information S1). The anomalous weakening of tropical upwelling is linked to downward transport of ozone-rich air from higher altitudes. Thus, the relatively small ozone losses in the lower stratosphere near 70 hPa are consistent with dynamical transport of ozone-rich air, partially offsetting the chemical ozone losses. Further interpretation of the dynamical responses to the nuclear war emissions is deferred to a future study.

The influence of using absolute versus relative ozone abundances on our interpretation of changes in ozone in the lower stratosphere was tested in Figures S7–S8 in Supporting Information S1. Both the absolute changes in ozone abundances and the chemical loss rates are small near ∼70 hPa (Figure S7–S8 in Supporting Information S1), while the relative differences in reaction rates in Figure 6b appear large because they are normalized by the smaller net loss rates from the **CTRL** experiment (Figure S8 in Supporting Information S1). Together, the results indicate that the effects of transport driven by the circulation anomalies are relatively larger in the lower stratosphere, due to the smaller chemical losses.

The rate of NO_x catalytic cycle is decreased to some extent, thus contributing to reduced ozone loss in the **IP-ALL** run (Figure 6b), whereas it is increased in the simulations by Bardeen et al. (2021). One of the main differences between their simulations and the **IP-ALL** simulations is the treatment of heterogeneous chemistry involving OC. Figure 7 illustrates the differences between the **IP-ALL** and **IP-ALL-xHET** runs, in (a) N_2O_5, (b) HNO_3, and (c) the heterogeneous reaction rate governing their conversion. These two simulations differ only in the implementation of the updated heterogeneous chemistry in OC; therefore, the results in Figure 7 exhibit the effects of this chemistry update. We find that the updated chemistry enhances the heterogeneous conversion of N_2O_5 to HNO_3, which leads to a reduction in NO_x concentrations and a subsequent decrease of the rate of the NO_x catalytic cycle.

The increase in the HO_x catalytic cycle shown in the **IP-ALL** run (Figure 6a) is due to enhanced HO_x concentrations (Figure 5f). This enhancement in HO_x is primarily driven by increased OH production resulting from enhanced water vapor abundances in the stratosphere. That is: As the smoke plume rises through the tropopause, it leads to substantial warming in the upper troposphere and lower stratosphere region, raising the cold point temperature (Figures 5a and 5b). This warming significantly enhances water vapor injected into the lower stratosphere, by up to ∼200% (Figure 5d). This additional stratospheric water vapor, in turn, increases HO_x concentrations through the production of OH. The chemical species and processes involved in HO_x production from enhanced stratospheric water vapor are also summarized in Figure 8.

3.3. Surface Climate Effects and Enhanced UV-B Radiation

A regional nuclear conflict is expected to induce a range of surface climate changes including global surface cooling, substantial reductions in precipitation, and increased UV-B radiation (Bardeen et al., 2021; Mills et al., 2014; Robock et al., 2007; Stenke et al., 2013; Toon et al., 2019). Additionally, such a conflict could have profound disruptions to food production, including both agriculture and fisheries (Jägermeyr et al., 2020; Scherrer et al., 2020; Xia et al., 2022; Xia & Robock, 2013). Here, we focus on the impacts of enhanced stratospheric ozone depletion in our simulations on surface UV-B radiation.

Figure 9 shows changes in surface UV-B radiation and column ozone for the **IP-ALL** experiment with respect to the **CTRL** experiment. The emissions from a nuclear war scenario have two opposing effects on surface UV-B

10.1029/2025EF006866

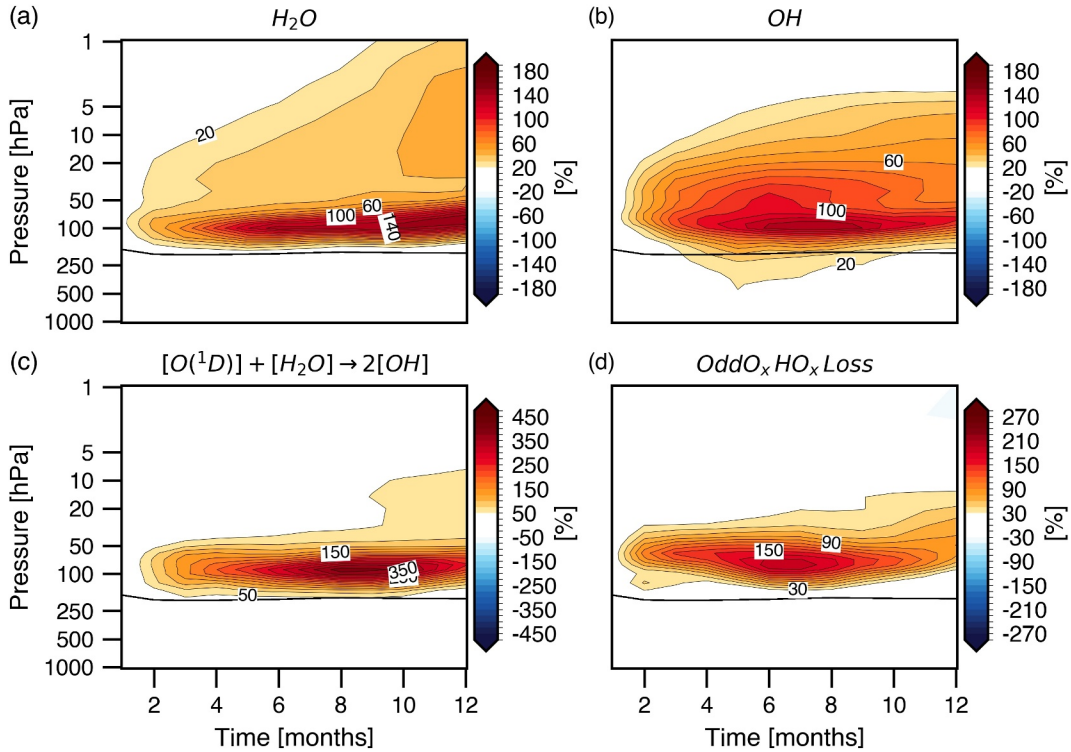

Figure 8. Changes in (a) H_2O, (b) OH, (c) OH production rate, and (d) odd-oxygen HO_x loss reaction rate between the **IP-ALL** and **CTRL** runs.

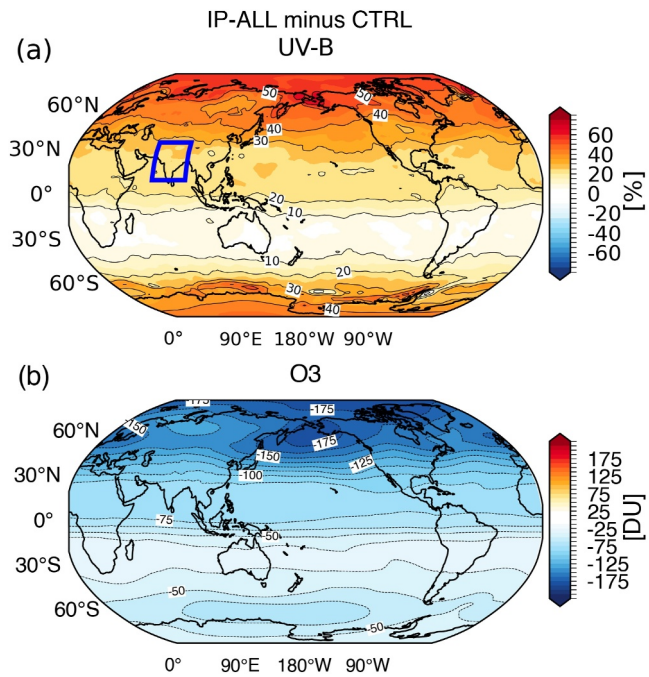

Figure 9. Changes in annual-mean (a) surface level UV-B radiation and (b) total column ozone during the first year, shown as differences between the **IP-ALL** and **CTRL** runs. The blue box in panel (a) marks the IP conflict region.

radiation: (a) the injected smoke particles can absorb a portion of UV-B, thereby reducing surface UV-B levels, while (b) stratospheric ozone depletion can increase surface UV-B, since ozone is also a major absorber of UV-B. Figure 9a reveals significant increases in UV-B radiation across the globe, which correspond closely with regions of substantial column ozone loss depicted in Figure 9b. This spatial correlation indicates that the changes in UV-B is primarily driven by ozone depletion. Thus, although smoke particles may absorb some UV-B, the much greater ozone loss results in a net increase in surface UV-B levels. These changes are evident globally, extending far beyond the conflict region (marked by the blue box in Figure 9a).

Elevated UV-B exposure has been linked to several harmful effects, such as cataract formation, DNA damage, sunburn, and skin cancer (MacKie, 2000; Madronich et al., 2021; Oriowo et al., 2001; Setlow, 1974). These health risks become more concerning given that, unlike ozone depletion from the total increase in manmade ozone depleting gases to date, very large ozone losses from a nuclear war are projected not only in polar regions but also in the mid-latitudes. Indeed, projected annual mean UV-B levels are estimated to increase by ∼50% over the NH mid-latitudes (Figure 9a), indicating a substantially greater risk of environmental damage and adverse health risks including skin cancer and cataracts in these densely populated regions.

4. Discussion and Conclusions

This study utilized a chemistry-climate model (WACCM4) to investigate the impacts of a regional-scale nuclear conflict, with a specific focus on its influence on the stratospheric ozone layer. Previous modeling studies of regional-scale nuclear exchanges have predicted that smoke emissions from such events could lead to global-scale ozone depletion. Building on this earlier research, our simulations for the first time include halogen emissions (chlorine and bromine) from urban fuels as well as an updated heterogeneous chemistry scheme that accounts for HCl solubility in OC.

Consistent with prior studies, the injection of 5 Tg of BC into the atmosphere leads to substantial calculated global stratospheric warming (up to ∼15 K), primarily due to shortwave radiation absorption by BC. More concerningly, our results show substantially amplified ozone depletion when both halogen emissions and the heterogeneous chemistry on organic aerosols are considered. While simulations without these additions suggest a global ozone burden decrease of approximately 20% (consistent with previous estimates), the inclusion of halogen emissions alone increased this to 25%. When both halogen emissions and the updated heterogeneous chemistry on organic aerosols were included, the peak global ozone loss increased to 37.5%. This represents a nearly twofold increase in relative ozone loss as our best estimate compared to previous simulations and demonstrates the key role of combined non-linear effects from the halogen emissions and the heterogeneous chemistry in driving stratospheric ozone depletion following a regional nuclear conflict. While there are substantial uncertainties in the amount of Cl and Br released in the burning of urban and wildland-urban areas, even a reduction in the Cl/Br input by 50% still led to substantially greater total ozone losses in our calculations than in previous work. Over the north polar regions, our simulations suggests that ozone depletion would be severe following a regional nuclear war, with peak losses reaching ∼80% of the total column, effectively creating an "Arctic ozone hole." The Arctic ozone hole occurs in every year of the 3 years of available simulation, and are linked to the assumed nuclear exchange in the relatively low latitudes of India and Pakistan through transport of halogens and smoke throughout the global stratosphere.

Our results reveal that significant ozone losses are not limited to the polar regions but also extend to the mid-latitudes (30–60°N), where total ozone depletion reaches 40%–60%. These widespread mid-latitude ozone losses are associated with large increases in surface UV-B levels (∼50%), substantially elevating the risk of environmental damage and adverse health effects in highly populated areas.

For future study, it would be important to investigate sensitivities across a broader range of nuclear conflict scenarios, incorporating different emission locations, composition (e.g., Cl/Br or OC/BC ratios) and altitudes of injection. Our findings also highlight the need for more accurate estimates of halogen emissions from urban fires. Additionally, extending simulations to better estimate the recovery timescales of both ozone and climate systems, and further analyses of the cascading impacts of severe ozone depletion on ecosystems and human health will also be critical.

In conclusion, our study provides a comprehensive analysis of the chemical impacts of a regional nuclear conflict on the stratospheric ozone layer. The incorporation of halogen emissions and heterogeneous chemistry on OC

aerosols leads to nearly twice the global ozone depletion previously predicted, with particularly severe ozone losses in the Arctic. We therefore view deepening our understanding of atmospheric chemistry under nuclear war scenarios as critical. The model improvements gained would also be valuable for accurately simulating other scenarios involving large injections of gases and aerosols from urban or wildland fires.

Conflict of Interest

The authors declare no conflicts of interest relevant to this study.

Data Availability Statement

The data used in the generation of the figures of this paper are available in Yook (2025). WACCM4 is an open-source community model, which was developed with support primarily from the National Science Foundation, see Marsh et al. (2013).

Acknowledgments
S. S and S. Y. are supported by a grant from the Future of Life Institute. The CESM project is supported primarily by the U.S. National Science Foundation. The authors acknowledge the Climate Simulation Laboratory at NCAR's Computational and Information Systems Laboratory (CISL; sponsored by NSF and other agencies) and the MIT's Massachusetts Green High Performance Computing Center (supported by the Center for Sustainability Science and Strategy) for providing computing and storage resources. Open Access funding enabled and organized by MIT Hybrid 2025. We thank the two anonymous reviewers for their helpful comments on the manuscript.

References

Alharbi, B. H., Pasha, M. J., & Al-Shamsi, M. A. S. (2021). Firefighter exposures to organic and inorganic gas emissions in emergency residential and industrial fires. *Science of the Total Environment*, *770*, 145332. https://doi.org/10.1016/j.scitotenv.2021.145332

Andreae, M. O. (2019). Emission of trace gases and aerosols from biomass burning–an updated assessment. *Atmospheric Chemistry and Physics*, *19*(13), 8523–8546. https://doi.org/10.5194/acp-19-8523-2019

Bardeen, C., Toon, O., Jensen, E., Marsh, D., & Harvey, V. (2008). Numerical simulations of the three-dimensional distribution of meteoric dust in the mesosphere and upper stratosphere. *Journal of Geophysical Research*, *113*(D17), D17202. https://doi.org/10.1029/2007jd009515

Bardeen, C. G., Garcia, R. R., Toon, O. B., & Conley, A. J. (2017). On transient climate change at the Cretaceous− Paleogene boundary due to atmospheric soot injections. *Proceedings of the National Academy of Sciences*, *114*(36), E7415–E7424. https://doi.org/10.1073/pnas.1708980114

Bardeen, C. G., Kinnison, D. E., Toon, O. B., Mills, M. J., Vitt, F., Xia, L., et al. (2021). Extreme ozone loss following nuclear war results in enhanced surface ultraviolet radiation. *Journal of Geophysical Research: Atmospheres*, *126*(18), e2021JD035079. https://doi.org/10.1029/2021jd035079

Blomqvist, P., & Simonson, M. (2009). Estimation of CO2-emissions from fires in dwellings, schools and cars in the Nordic countries. In.

Blomqvist, P., Simonson McNamee, M., Stec, A. A., Gylestam, D., & Karlsson, D. (2010). Characterisation of fire generated particles: BRANDFORSK project 700-061, FireTechnology, SP Report 2010.

Brasseur, G. P., & Solomon, S. (2005). *Aeronomy of the middle atmosphere: Chemistry and physics of the stratosphere and mesosphere*. Springer.

Butler, K. M., & Mulholland, G. W. (2004). Generation and transport of smoke components. *Fire Technology*, *40*(2), 149–176. https://doi.org/10.1023/b:fire.0000016841.07530.64

Christian, T. J., Yokelson, R., Cárdenas, B., Molina, L. T., Engling, G., & Hsu, S.-C. (2010). Trace gas and particle emissions from domestic and industrial biofuel use and garbage burning in central Mexico. *Atmospheric Chemistry and Physics*, *10*(2), 565–584. https://doi.org/10.5194/acp-10-565-2010

Coupe, J., Bardeen, C. G., Robock, A., & Toon, O. B. (2019). Nuclear winter responses to nuclear war between the United States and Russia in the whole atmosphere community climate model version 4 and the Goddard Institute for Space Studies ModelE. *Journal of Geophysical Research: Atmospheres*, *124*(15), 8522–8543. https://doi.org/10.1029/2019jd030509

Crutzen, P. J., & Birks, J. W. (2016). The atmosphere after a nuclear war: Twilight at noon. *Paul J. Crutzen: A Pioneer on Atmospheric Chemistry and Climate Change in the Anthropocene*, 125–152. https://doi.org/10.1007/978-3-319-27460-7_5

Davis, S. C., & Boundy, R. G. (2021). Transportation energy data book (Edition 39).

Dod, R., Brown, N., Mowrer, F., Novakov, T., & Williamson, R. (1989). Smoke emission factors from medium-scale fires: Part 2. *Aerosol science and technology*, *10*(1), 20–27. https://doi.org/10.1080/02786828908959217

Gann, R. G., Averill, J. D., Johnsson, E. L., Nyden, M. R., & Peacock, R. D. (2010). Fire effluent component yields from room-scale fire tests. *Fire and Materials*, *34*(6), 285–314. https://doi.org/10.1002/fam.1024

Garcia, R. R., Smith, A. K., Kinnison, D. E., Cámara, Á. d. l., & Murphy, D. J. (2017). Modification of the gravity wave parameterization in the Whole Atmosphere Community Climate Model: Motivation and results. *Journal of the Atmospheric Sciences*, *74*(1), 275–291. https://doi.org/10.1175/jas-d-16-0104.1

Glasstone, S., & Dolan, P. (1977). Biological effects. In *The effects of nuclear weapons* (pp. 541–559).

Griffiths, S. D., Entwistle, J. A., Kelly, F. J., & Deary, M. E. (2022). Characterising the ground level concentrations of harmful organic and inorganic substances released during major industrial fires, and implications for human health. *Environment International*, *162*, 107152. https://doi.org/10.1016/j.envint.2022.107152

Holder, A. L., Ahmed, A., Vukovich, J. M., & Rao, V. (2023). Hazardous air pollutant emissions estimates from wildfires in the wildland urban interface. *PNAS Nexus*, *2*(6), pgad186. https://doi.org/10.1093/pnasnexus/pgad186

Hurrell, J. W., Holland, M. M., Gent, P. R., Ghan, S., Kay, J. E., Kushner, P. J., et al. (2013). The community earth system model: A framework for collaborative research. *Bulletin of the American Meteorological Society*, *94*(9), 1339–1360. https://doi.org/10.1175/bams-d-12-00121.1

Jägermeyr, J., Robock, A., Elliott, J., Müller, C., Xia, L., Khabarov, N., et al. (2020). A regional nuclear conflict would compromise global food security. *Proceedings of the National Academy of Sciences*, *117*(13), 7071–7081. https://doi.org/10.1073/pnas.1919049117

Jensen, E., & Pfister, L. (2004). Transport and freeze-drying in the tropical tropopause layer. *Journal of Geophysical Research*, *109*(D2), D02207. https://doi.org/10.1029/2003jd004022

Kinnison, D., Brasseur, G. P., Walters, S., Garcia, R., Marsh, D., Sassi, F., et al. (2007). Sensitivity of chemical tracers to meteorological parameters in the MOZART-3 chemical transport model. *Journal of Geophysical Research*, *112*(D20), D20302. https://doi.org/10.1029/2006jd007879

Lewis, K. N. (1979). The prompt and delayed effects of nuclear war. *Scientific American*, *241*(1), 35–47. https://doi.org/10.1038/scientificamerican0779-35

Li, T., Chen, H., Fung, J. C., Chan, D. H., Yu, A. L., Leung, K. K., & Yu, J. Z. (2023). Large presence of bromine and toxic metals in ambient fine particles from urban fires. *Atmospheric Environment*, *295*, 119554. https://doi.org/10.1016/j.atmosenv.2022.119554

Lönnermark, A., & Blomqvist, P. (2006). Emissions from an automobile fire. *Chemosphere*, *62*(7), 1043–1056. https://doi.org/10.1016/j.chemosphere.2005.05.002

MacKie, R. (2000). Effects of ultraviolet radiation on human health. *Radiation Protection Dosimetry*, *91*(1–3), 15–18. https://doi.org/10.1093/oxfordjournals.rpd.a033186

Madronich, S., & Flocke, S. (1997). Theoretical estimation of biologically effective UV radiation at the Earth's surface. In C. Zerefos (Ed.), *Solar ultraviolet radiation-modeling, measurements and effects. NATO ASI Ser* (Vol. I52, pp. 23–48). Springer. https://doi.org/10.1007/978-3-662-03375-3_3

Madronich, S., Lee-Taylor, J. M., Wagner, M., Kyle, J., Hu, Z., & Landolfi, R. (2021). Estimation of skin and ocular damage avoided in the United States through implementation of the montreal protocol on substances that deplete the ozone layer. *ACS Earth and Space Chemistry*, *5*(8), 1876–1888. https://doi.org/10.1021/acsearthspacechem.1c00183

Marsh, D. R., Mills, M. J., Kinnison, D. E., Lamarque, J.-F., Calvo, N., & Polvani, L. M. (2013). Climate change from 1850 to 2005 simulated in CESM1 (WACCM). *Journal of Climate*, *26*(19), 7372–7391. https://doi.org/10.1175/jcli-d-12-00558.1

Mills, M. J., Toon, O. B., Lee-Taylor, J., & Robock, A. (2014). Multidecadal global cooling and unprecedented ozone loss following a regional nuclear conflict. *Earth's Future*, *2*(4), 161–176. https://doi.org/10.1002/2013ef000205

Mills, M. J., Toon, O. B., Turco, R. P., Kinnison, D. E., & Garcia, R. R. (2008). Massive global ozone loss predicted following regional nuclear conflict. *Proceedings of the National Academy of Sciences*, *105*(14), 5307–5312. https://doi.org/10.1073/pnas.0710058105

National Academies of Sciences, Engineering, and Medicine. et al., (2022). *The chemistry of fires at the wildland-urban interface*. Washington, DC: The National Academies Press. https://doi.org/10.17226/26460

National Resource Council. (1985). *The effects on the atmosphere of a major nuclear exchange*. National Academy Press.

Ni, H.-G., Lu, S.-Y., Mo, T., & Zeng, H. (2016). Brominated flame retardant emissions from the open burning of five plastic wastes and implications for environmental exposure in China. *Environmental Pollution*, *214*, 70–76. https://doi.org/10.1016/j.envpol.2016.03.049

Oriowo, O. M., Cullen, A. P., Chou, B. R., & Sivak, J. G. (2001). Action spectrum and recovery for in vitro UV-induced cataract using whole lenses. *Investigative Ophthalmology & Visual Science*, *42*(11), 2596–2602.

Peterson, D. A., Fromm, M. D., McRae, R. H., Campbell, J. R., Hyer, E. J., Taha, G., et al. (2021). Australia's Black Summer pyrocumulonimbus super outbreak reveals potential for increasingly extreme stratospheric smoke events. *npj Climate and Atmospheric Science*, *4*(1), 38. https://doi.org/10.1038/s41612-021-00192-9

Pittock, A. B., Ackerman, T. P., Crutzen, P. J., MacCracken, M. C., & Shapiro, C. S. (1985). Environmental consequences of nuclear war.

Reisen, F., Bhujel, M., & Leonard, J. (2014). Particle and volatile organic emissions from the combustion of a range of building and furnishing materials using a cone calorimeter. *Fire Safety Journal*, *69*, 76–88. https://doi.org/10.1016/j.firesaf.2014.08.008

Reisner, J., D'Angelo, G., Koo, E., Even, W., Hecht, M., Hunke, E., et al. (2018). Climate impact of a regional nuclear weapons exchange: An improved assessment based on detailed source calculations. *Journal of Geophysical Research: Atmospheres*, *123*(5), 2752–2772. https://doi.org/10.1002/2017jd027331

Robock, A. (1984). Snow and ice feedbacks prolong effects of nuclear winter. *Nature*, *310*(5979), 667–670. https://doi.org/10.1038/310667a0

Robock, A., Oman, L., & Stenchikov, G. L. (2007). Nuclear winter revisited with a modern climate model and current nuclear arsenals: Still catastrophic consequences. *Journal of Geophysical Research*, *112*(D13), D13107. https://doi.org/10.1029/2006jd008235

Scherrer, K. J., Harrison, C. S., Heneghan, R. F., Galbraith, E., Bardeen, C. G., Coupe, J., et al. (2020). Marine wild-capture fisheries after nuclear war. *Proceedings of the National Academy of Sciences*, *117*(47), 29748–29758. https://doi.org/10.1073/pnas.2008256117

Setlow, R. B. (1974). The wavelengths in sunlight effective in producing skin cancer: A theoretical analysis. *Proceedings of the National Academy of Sciences*, *71*(9), 3363–3366. https://doi.org/10.1073/pnas.71.9.3363

Shi, Q., Jayne, J., Kolb, C., Worsnop, D., & Davidovits, P. (2001). Kinetic model for reaction of ClONO2 with H2O and HCl and HOCl with HCl in sulfuric acid solutions. *Journal of Geophysical Research*, *106*(D20), 24259–24274. https://doi.org/10.1029/2000jd000181

Solomon, S. (1999). Stratospheric ozone depletion: A review of concepts and history. *Reviews of Geophysics*, *37*(3), 275–316. https://doi.org/10.1029/1999rg900008

Solomon, S., Stone, K., Yu, P., Murphy, D., Kinnison, D., Ravishankara, A., & Wang, P. (2023). Chlorine activation and enhanced ozone depletion induced by wildfire aerosol. *Nature*, *615*(7951), 259–264. https://doi.org/10.1038/s41586-022-05683-0

Stenke, A., Hoyle, C. R., Luo, B., Rozanov, E., Gröbner, J., Maag, L., et al. (2013). Climate and chemistry effects of a regional scale nuclear conflict. *Atmospheric Chemistry and Physics*, *13*(19), 9713–9729. https://doi.org/10.5194/acp-13-9713-2013

Stone, K., Solomon, S., Yu, P., Murphy, D. M., Kinnison, D., & Guan, J. (2025). Two-years of stratospheric chemistry perturbations from the 2019–2020 Australian wildfire smoke. *Atmospheric Chemistry and Physics*, *25*(14), 7683–7697. https://doi.org/10.5194/acp-25-7683-2025

Szewczyński, K. (2023). Spatial analysis of the impact of motor vehicle fires on the urban environment using the example of Warsaw. *Architecture Civil Engineering Environment*, *16*(3), 181-–191. https://doi.org/10.2478/acee-2023-0045

Toon, O. B., Bardeen, C. G., Robock, A., Xia, L., Kristensen, H., McKinzie, M., et al. (2019). Rapidly expanding nuclear arsenals in Pakistan and India portend regional and global catastrophe. *Science Advances*, *5*(10), eaay5478. https://doi.org/10.1126/sciadv.aay5478

Toon, O. B., Robock, A., Turco, R. P., Bardeen, C., Oman, L., & Stenchikov, G. L. (2007). Consequences of regional-scale nuclear conflicts. In *Science* (Vol. 315(5816), pp. 1224–1225). https://doi.org/10.1126/science.1137747. American Association for the Advancement of Science.

Toon, O. B., Turco, R., Westphal, D., Malone, R., & Liu, M. (1988). A multidimensional model for aerosols: Description of computational analogs. *Journal of the Atmospheric Sciences*, *45*(15), 2123–2144. https://doi.org/10.1175/1520-0469(1988)045<2123:ammfad>2.0.co;2

Turco, R. P., Toon, O. B., Ackerman, T. P., Pollack, J. B., & Sagan, C. (1983). Nuclear winter: Global consequences of multiple nuclear explosions. *Science*, *222*(4630), 1283–1292. https://doi.org/10.1126/science.222.4630.1283

Wagman, B. M., Lundquist, K. A., Tang, Q., Glascoe, L. G., & Bader, D. C. (2020). Examining the climate effects of a regional nuclear weapons exchange using a multiscale atmospheric modeling approach. *Journal of Geophysical Research: Atmospheres*, *125*(24), e2020JD033056. https://doi.org/10.1029/2020jd033056

Wang, S., Bathras, B. L., Cui, W., Milazzo, M., Goldstein, A. H., & Gollner, M. J. (2025). Laboratory quantification of emissions from wildland-urban interface fuels using fourier-transform Infrared Spectroscopy. *Environmental Science & Technology*, *59*(25), 12843–12852. https://doi.org/10.1021/acs.est.5c03514

Weimer, M., Wilka, C., Kinnison, D., Garcia, R., Bacmeister, J., Alexander, M., et al. (2023). A method for estimating global subgrid-scale orographic gravity-wave temperature perturbations in chemistry-climate models. *Journal of Advances in Modeling Earth Systems*, *15*(9), e2022MS003505. https://doi.org/10.1029/2022ms003505

Wolf, E. T., & Toon, O. B. (2010). Fractal organic hazes provided an ultraviolet shield for early Earth. *Science*, *328*(5983), 1266–1268. https://doi.org/10.1126/science.1183260

Xia, L., & Robock, A. (2013). Impacts of a nuclear war in South Asia on rice production in mainland China. *Climatic Change*, *116*(2), 357–372. https://doi.org/10.1007/s10584-012-0475-8

Xia, L., Robock, A., Scherrer, K., Harrison, C., Jaegermeyr, J., Bardeen, C., et al. (2021). Global famine after nuclear War.

Xia, L., Robock, A., Scherrer, K., Harrison, C. S., Bodirsky, B. L., Weindl, I., et al. (2022). Global food insecurity and famine from reduced crop, marine fishery and livestock production due to climate disruption from nuclear war soot injection. *Nature Food*, *3*(8), 586–596. https://doi.org/10.1038/s43016-022-00573-0

Yook, S. (2025). Replication data for: Figures in Arctic Ozone Holes and Enhanced Mid-Latitude Ozone Losses Due to Halogen Chemistry Following a Regional Nuclear Conflict [Dataset]. *Harvard Dataverse*. https://doi.org/10.7910/DVN/MAOT5G

Yu, P., Davis, S. M., Toon, O. B., Portmann, R. W., Bardeen, C. G., Barnes, J. E., et al. (2021). Persistent stratospheric warming due to 2019–2020 Australian wildfire smoke. *Geophysical Research Letters*, *48*(7), e2021GL092609. https://doi.org/10.1029/2021gl092609

Zhang, B., Shen, H., Yun, X., Zhong, Q., Henderson, B. H., Wang, X., et al. (2022). Global emissions of hydrogen chloride and particulate chloride from continental sources. *Environmental Science & Technology*, *56*(7), 3894–3904. https://doi.org/10.1021/acs.est.1c05634